AIP Applied Physics Letters

Switching mechanism of double forming process phenomenon in ZrOx/HfOy bilayer resistive switching memory structure with large endurance

Chun-Yang Huang, Chung-Yu Huang, Tsung-Ling Tsai, Chun-An Lin, and Tseung-Yuen Tseng

Citation: Applied Physics Letters **104**, 062901 (2014); doi: 10.1063/1.4864396
View online: http://dx.doi.org/10.1063/1.4864396
View Table of Contents: http://scitation.aip.org/content/aip/journal/apl/104/6?ver=pdfcov
Published by the AIP Publishing

Articles you may be interested in
Low power W:AlOx/WOx bilayer resistive switching structure based on conductive filament formation and rupture mechanism
Appl. Phys. Lett. **102**, 173503 (2013); 10.1063/1.4803462

Mechanism of resistive switching in Cu/AlOx/W nonvolatile memory structures
J. Appl. Phys. **113**, 164506 (2013); 10.1063/1.4803062

Resistive switching mechanisms relating to oxygen vacancies migration in both interfaces in Ti/HfOx/Pt memory devices
J. Appl. Phys. **113**, 064510 (2013); 10.1063/1.4791695

Robust unipolar resistive switching of Co nano-dots embedded ZrO2 thin film memories and their switching mechanism
J. Appl. Phys. **111**, 014505 (2012); 10.1063/1.3674322

Effect of ZrO x / HfO x bilayer structure on switching uniformity and reliability in nonvolatile memory applications
Appl. Phys. Lett. **97**, 172105 (2010); 10.1063/1.3491803

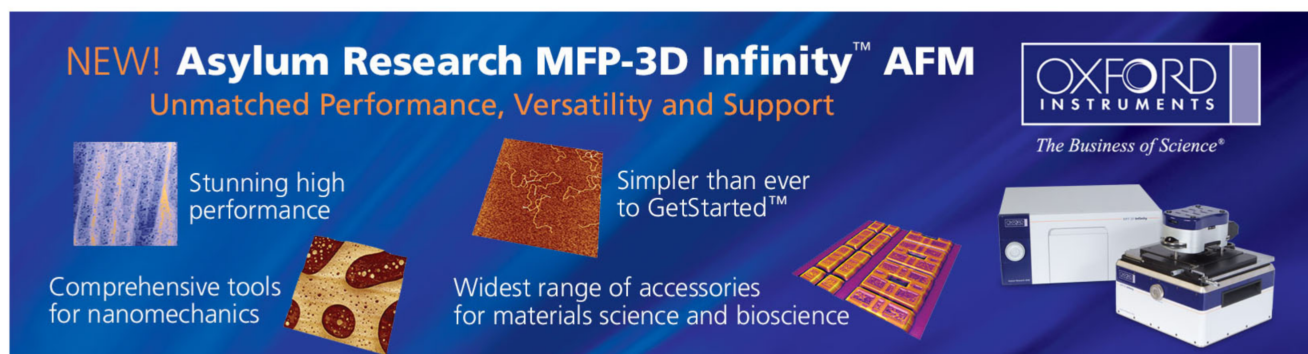

This article is copyrighted as indicated in the article. Reuse of AIP content is subject to the terms at: http://scitation.aip.org/termsconditions. Downloaded to IP: 140.113.38.11 On: Fri, 02 May 2014 03:55:39

APPLIED PHYSICS LETTERS **104**, 062901 (2014)

Switching mechanism of double forming process phenomenon in ZrO_x/HfO_y bilayer resistive switching memory structure with large endurance

Chun-Yang Huang, Chung-Yu Huang, Tsung-Ling Tsai, Chun-An Lin, and Tseung-Yuen Tseng[a]

Department of Electronics Engineering and Institute of Electronics, National Chiao Tung University, Hsinchu 30010, Taiwan

(Received 6 November 2013; accepted 24 January 2014; published online 10 February 2014)

In this Letter, the mechanism of double forming process phenomenon revealing in ZrO_2/HfO_2 bilayer resistive random access memory structure is investigated. This phenomenon caused by the formation of TiON interfacial layer can be well explained by using the energy band diagram. The TiON interfacial layer will be a tunneling barrier during the first forming process when a negative voltage applied on the device, while it will breakdown when applying a positive voltage. Besides, due to the double forming process, an asymmetric conductive filament with narrower size at ZrO_2/HfO_2 interface is formed in the device. The point for formation and rupture of the conductive filament can be confined at the ZrO_2/HfO_2 interface, and it will suppress the consumption of oxygen ions during endurance test. Therefore, high speed (40 ns) and large endurance (10^7 cycles) characteristics are achieved in this device structure. © *2014 AIP Publishing LLC*. [http://dx.doi.org/10.1063/1.4864396]

Transition metal oxide (TMO) based resistive random access memory (RRAM) is one of the promising candidates to replace the current flash memory device as the next-generation nonvolatile memory application.[1,2] The resistive switching (RS) phenomenon in metal oxide layer is attributed to the conductive filament consisting of migrated oxygen vacancies or ions under the applied electric field.[3–6] Recently, the bilayer structure RRAM devices were proposed to improve endurance property, which revealed high performance RS than single layer devices.[7–11] However, the resistance ratio between high resistance state (HRS) and low resistance state (LRS) will tend to fluctuation and decreasing during switching cycles test.[12,13] This problem leads the endurance degradation for its applications. Some literature reported that the endurance degradation is caused by the consumption of available oxygen ions for participating in RS, which may be caused by the oxygen ions migrating toward electrodes and release them from the electrodes under an applying electric field.[14–18]

In this study, a $TaN/ZrO_2/HfO_2/TiN$ RRAM device was proposed for the high performance RS properties. All of those materials for making metal-insulator-metal structure were compatible with complementary metal oxide semiconductor (CMOS) processes. In addition, we found that those devices cannot execute success resistance switching after forming process by applying a positive voltage. In addition, an interesting phenomenon of the double forming process was found in this bilayer structure. The conductive filament mechanism can be used to well explain the double forming process phenomenon. It was clearly indicated that the endurance fluctuation can be improved by controlling the point in the interface between HfO_2 and ZrO_2 layers for formation and rupture of conductive filament. By the way, large endurance cycles (10^7 cycles) with about 100 times of HRS/LRS ratio under a fast speed (40 ns) were achieved in this $TaN/ZrO_2/HfO_2/TiN$ device structure.

A 5 nm HfO_2 thin film as 1st RS layer was deposited on TiN bottom electrode by sputtering at room temperature in 5 mTorr atmosphere with Ar/O_2 mixture gas ratio of 10:3. Subsequently, an oxygen annealing process at a furnace of 400 °C with O_2 gas flow of 30 SCCM for 30 min was executed to improve the quality and reduce the amount of defects (oxygen vacancies) in HfO_2 layer. Then, a 3 nm ZrO_2 thin film as 2nd RS layer was deposited by sputtering at room temperature in 10 mTorr atmosphere with Ar/O_2 mixture gas ratio of 2:1. Finally, a 100 nm TaN top electrode with a diameter of 150 μm was deposited by sputtering at room temperature to form the $TaN/ZrO_2/HfO_2/TiN$ architecture. The direct current (DC) electrical characteristics measurements were performed by using an Agilent B1500A semiconductor parameter analyzer, and the alternating current (AC) pulse was generated by Agilent B1530A waveform generator/fast measurement unit (WGFMU). The voltage was applied on the TaN top electrode with the TiN bottom electrode grounded.

Figure 1(a) shows the typical cross-section transmission electron microscopy (TEM) image of the $TaN/ZrO_2/HfO_2/TiN$ bilayer RRAM device. Due to the obviously crystalline orientation formed in the TiN electrode, a thin interfacial layer TiON (~2 nm) is observed. The DC sweep electrical I-V curve of the present device is shown in Fig. 1(b). Unlike regular bipolar RRAM devices, the $TaN/ZrO_2/HfO_2/TiN$ device reveals the double forming process phenomenon for switching its resistance from initial state (IS) to LRS. The double forming process can be well described in six steps: (1) First forming process, (2) Medium state (denoted as MS), (3) Second forming process, (4) LRS, (5) Reset process, and (6) HRS, as shown in Fig. 1(b).

Step (1) is to construct a larger size conductive filament in ZrO_2 layer and a thinner one in HfO_2 layer. The typical X-ray photoelectron spectra (XPS) analyses can confirm this

[a]Email: tseng@cc.nctu.edu.tw

This article is copyrighted as indicated in the article. Reuse of AIP content is subject to the terms at: http://scitation.aip.org/termsconditions. Downloaded to IP: 140.113.38.11 On: Fri, 02 May 2014 03:55:39

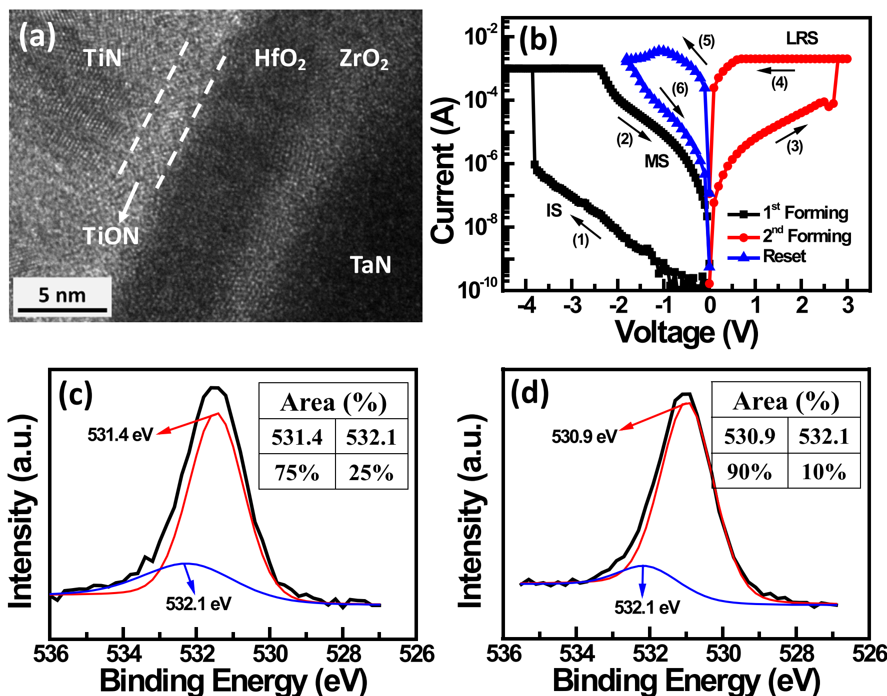

FIG. 1. (a) Typical cross-section TEM image of the TaN/ZrO_2/HfO_2/TiN RRAM device. (b) DC sweep I-V curve of the double forming process phenomenon: (1) First forming process; (2) Medium state; (3) Second forming process; (4) Low resistance state; (5) Reset process; and (6) High resistance state. The O 1 s XPS spectra of (c) ZrO_2 and (d) HfO_2 layers.

phenomenon. The oxygen compositions of ZrO_2 and HfO_2 layers are depicted in Figs. 1(c) and 1(d), respectively. The two major peaks in these figures can be fitted for ZrO_2 and HfO_2 layers, respectively. The binding energies of the main peaks at around 531.4 and 530.9 eV are attributed to the O^{2-} ions in the stoichiometric Zr-O and Hf-O bonds, respectively, while the higher energies of 532.1 eV in these figures correspond to the oxygen vacancies in ZrO_2 and HfO_2 layers, respectively.[19] The inset tables in Figs. 1(c) and 1(d) indicate the area proportion of each peak. Due to the post oxygen annealing process treated for the HfO_2 layer, the percentage of oxygen vacancies existed in the HfO_2 layer is only 10%, whereas that in the ZrO_2 layer is 25%. Therefore, compared to ZrO_2 layer, less amount of the oxygen vacancies is stored in HfO_2 layer, as shown in Fig. 2(a). Besides, in our previous study, the physical size of the conductive filament in an oxygen vacancies deficient layer is narrower than that in the oxygen vacancies rich layer.[9] Therefore, two different sizes of conductive filaments are formed and linked together to connect top electrode and TiON layer (Fig. 2(b)). However, no conductive filament is formed within the TiON layer in the step (1). It can be explained by the energy band diagram shown in Figs. 2(f)–2(h). Fig. 2(f) depicts the conduction band offset diagram. As a lot of defects (oxygen vacancies) exist in the ZrO_2 layer, the electrons can easily hop through it from top electrode to HfO_2 layer when a negative voltage is applied. Therefore, when the applied negative voltage increases to the first forming voltage (−4 V), the defects (oxygen vacancies) generate and form conductive filament in HfO_2 layer. According to the band diagram in Fig. 2(g), the electron passing through HfO_2 layer can easily slip along the tilted conduction band in TiON layer to TiN bottom electrode. Therefore, a larger current reaches to compliance current as measured in Fig. 1(b). However, the energy band will tend to be more flat when the applied voltage sweeps back to 0 V, thus the electrons located at the defects of HfO_2 layer will face a barrier between HfO_2 and TiON layers. This barrier causes a larger resistance when decreasing the applying

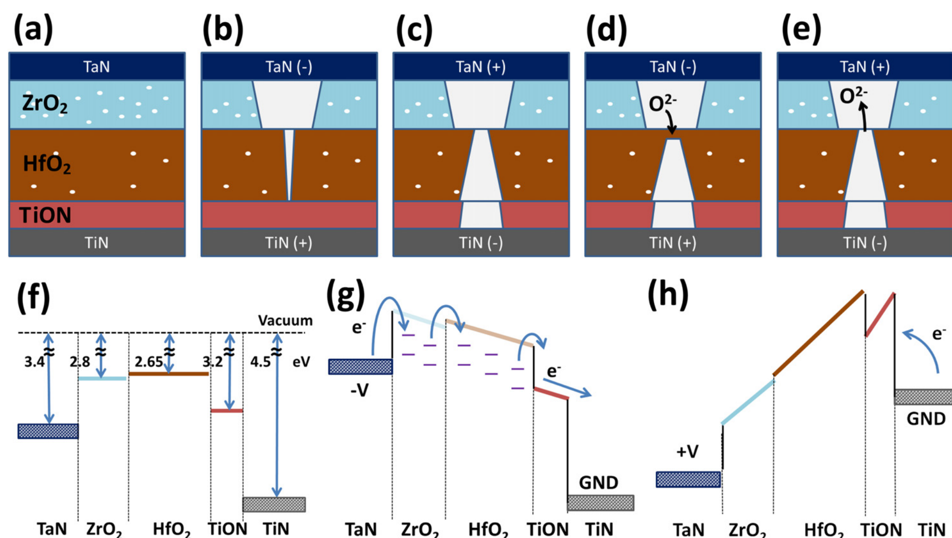

FIG. 2. Schematic description of the conducting mechanism of the double forming process of the TaN/ZrO_2/HfO_2/TiN RRAM device on (a) initial state, (b) first forming process, (c) second forming process, (d) reset process, and (e) set process. The energy band diagram at (f) conduction band offset, (g) applying a negative voltage, and (h) applying a positive voltage on the top electrode in the present device. The work functions of TaN (3.4 eV) and TiN (4.5 eV); the electron affinities of ZrO_2 (2.8 eV), HfO_2 (2.65 eV), and TiON (3.2 eV) are found in Refs. 21–24.

This article is copyrighted as indicated in the article. Reuse of AIP content is subject to the terms at: http://scitation.aip.org/termsconditions. Downloaded to IP: 140.113.38.11 On: Fri, 02 May 2014 03:55:39

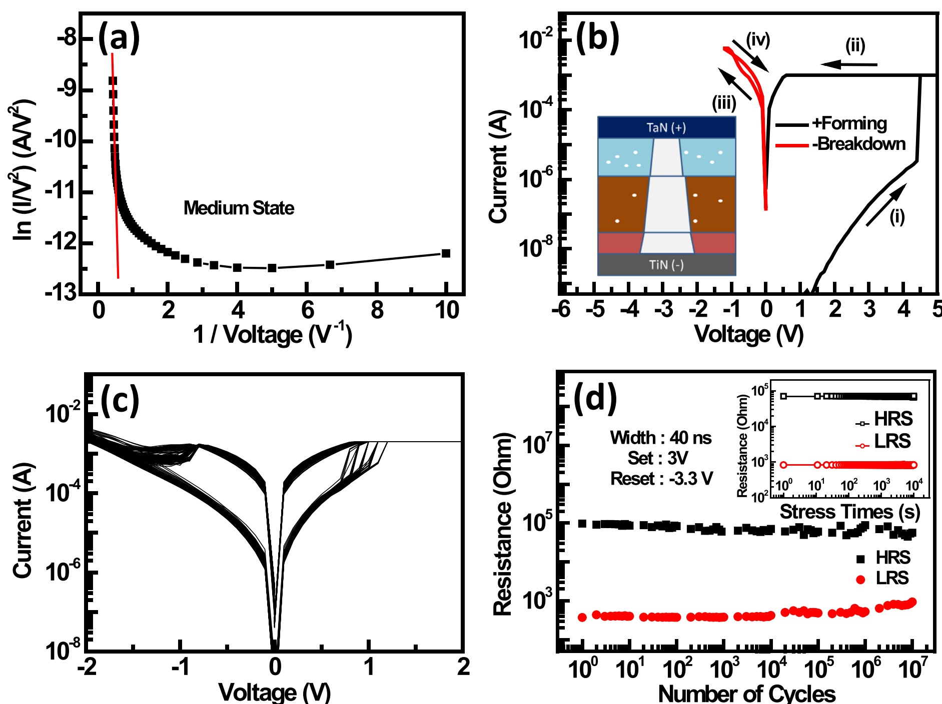

FIG. 3. (a) F-N tunneling curve fitting of the TaN/ZrO_2/HfO_2/TiN RRAM device in medium state. (b) I–V curve of positive voltage forming process. The inset shows the schematic diagram. (c) Typical bipolar I-V curves with 100 times switching cycles. (d) AC endurance characteristic at room temperature and the inset shows the read disturbance behavior at 85 °C with a read voltage at 0.3 V of the device.

voltage. Therefore, the device switches from IS to MS except regular LRS in step (2), and the conductive mechanism is dominated by the Fowler-Nordheim (FN) tunneling.[20] In addition, the $\ln(I/V^2)$ versus 1/V curve shows a straight fitting line with a negative slope at large voltage region (more negative) in HRS, which proves the conductive mechanism dominated by FN tunneling in step (2), as shown in Fig. 3(a). The property in step (2) is also shown in the HfO_2 single layer device; however, no further RS behavior reveals in it (not shown here).

Besides, compared to the TaN/ZrO_2/HfO_2/TiN device under the double forming process in Fig. 1(b), the another same fresh device can also execute a single forming process by applying a positive voltage. However, if we attempt to switch such a device from LRS to HRS by applying a negative bias, the device switches to much lower resistive LRS rather than switches to HRS, as shown in curves (iii) and (iv) of Fig. 3(b). Fig. 2(h) illustrates the energy band diagram of positive forming process induced hard breakdown. Due to the asymmetric barriers at TiN/TiON (1.3 eV) and TaN/ZrO_2 (0.6 eV) interfaces, the higher barrier at TiN/TiON interface causes that the FN tunneling phenomenon in TiON is not obvious during the positive forming process. On the other hand, due to the work function difference between TaN and TiN electrodes, there is a build-in electric field created from TaN toward TiN in the resistive switching layers. When a positive voltage is applied on the TaN top electrode, the external electric field associated with build-in one will enhance the effective field in the layers. Therefore, the TiON layer will tend to breakdown and generate more oxygen vacancies in it during the positive forming process. On the other hand, oxygen vacancies also generate in HfO_2 layer in this situation. Those oxygen vacancies will tend to migrate to form the conductive filament. The shape of the conductive filament is illustrated in inset of the Fig. 3(b). Therefore, the device cannot switch to HRS because of a large sized conductive filament formed. Those results demonstrate that the TaN/ZrO_2/HfO_2/TiN device cannot operate suitably under a single positive forming process.

After completing the first forming process, we also try a negative voltage to switch the device from MS to a much higher resistance state; unfortunately, a permanent hard breakdown occurs in it. On the other hand, a successful resistance switching for memory property is executed when a positive voltage applies on the device in MS as shown in Fig. 1(b). The successful bipolar RS characteristic with 100 cycles is shown in Fig. 3(c). Compared to the smaller set voltage ($\sim$1 V) in Fig. 3(c), a larger threshold voltage about 2.8 V is measured. Therefore, we call this process as the second forming process with a second forming voltage of 2.8 V in step (3) of Fig. 1(b). After the second forming process, the device can switch from MS to LRS, as shown in step (4). Finally, the regular reset process is effectively executed by applying a negative voltage after the double forming process steps in the present device, as shown in steps (5) and (6). Due to a positive voltage applies on the top electrode, the oxygen vacancies with positive charge in HfO_2 layer will be repelled toward bottom electrode. By the way, as described before in Figs. 2(h) and 3(b), a positive voltage applied on the device will cause a breakdown in the TiON layer. Therefore, the conductive filament will re-construct itself to a large size at near TiN and a small size at near the ZrO_2/HfO_2 interface. Besides, the size of conductive filament in ZrO_2 layer is still large because of the existing large amount of oxygen vacancies in it during step (1). Hence, an asymmetric shape of conductive filament with a weakest point located at the ZrO_2/HfO_2 interface is designed and formed in the present device, as shown in Fig. 2(c). Thus, the device switches from MS to LRS due to the formation of complete conductive filament. Finally, the repeatable resistance switching properties can be achieved in this device.

The electric field can be enhanced in the conductive filament due to its larger conductivity than other regions of the device. During the reset process, the interstitially oxygen

This article is copyrighted as indicated in the article. Reuse of AIP content is subject to the terms at: http://scitation.aip.org/termsconditions. Downloaded to IP: 140.113.38.11 On: Fri, 02 May 2014 03:55:39

ions existed in ZrO_2 layer will migrate to HfO_2 layer when a negative voltage is applied on top electrode. In addition, the current flowing through the narrowest size of asymmetric conductive filament (the ZrO_2/HfO_2 interface) will cause a serious local Joule heating in it. Consequently, the migrated oxygen ions associated with local thermal effect will easily recombine (oxidation) with oxygen vacancies at the ZrO_2/HfO_2 interface or top of the conductive filament in HfO_2 layer. Thus, dissolution of the asymmetric conductive filament causes it switching from LRS to HRS, as shown in Fig. 2(d). On the other hand, when a positive voltage is applied on the device in Fig. 2(c), the oxygen ions existed in HfO_2 layer will also tend to migrate to ZrO_2 layer. However, compared to HfO_2 layer, the conductive filament in ZrO_2 layer is too large to rupture it. Therefore, the device cannot switch to HRS by applying a positive voltage on it. When a positive voltage is applied on it during the set process, a soft breakdown and reduction reaction (oxygen vacancies are generated) occur in the region above top of the conduction filament in HfO_2 layer. The escaped oxygen ions due to generated oxygen vacancies migrate back to ZrO_2 layer to oxidize part of the oxygen vacancies to re-form the conductive filament. The device switches back to LRS, as shown in Fig. 2(e). Therefore, the formation and rupture point of conductive filament for RS property can be limited at a very narrow region at the ZrO_2/HfO_2 interface.

Due to the oxygen vacancies generation and recombination can be confined at the ZrO_2/HfO_2 interface except near the electrode during RS cycles test, the problem of escaping oxygen ions from electrodes[18] can be suppressed in the device. Therefore, it can be expected that the highly stable endurance characteristic can be achieved in the present device structure. Fig. 3(d) shows the high speed AC endurance property by using a pulse height of 3 V for set process and −3.3 V for reset process under a pulse width of 40 ns. Large endurance of more than 10^7 switching cycles is achieved. About 100 times resistance ratio with less fluctuation between HRS and LRS is revealed in the ZrO_2/HfO_2 bilayer device. In addition, the read disturbance property under a constant voltage stress of 0.3 V at 85 °C is shown in the inset of Fig. 3(d). No degradation property in both HRS and LRS is maintained for more than 10^4 s.

In summary, the $TaN/ZrO_2/HfO_2/TiN$ bilayer RRAM structure is fabricated in this study. The structure reveals the double forming process phenomenon before resistive switching cycles. The energy band diagram and conductive filament model can well explain this interesting phenomenon. Due to the formation of TiON thin layer between HfO_2 and TiN interface, it causes a dielectric breakdown only by using positive voltage applied on the device. An asymmetric conductive filament is formed after the double forming process, which can confine the point for formation and rupture of conductive filament at the ZrO_2/HfO_2 interface during resistive switching. It can suppress the resistance state degradation caused by escaping the oxygen ions from the electrodes. Therefore, the large endurance (10^7 cycles) with high operation speed (40 ns) is observed in this device structure, which is a good candidate for next generation nonvolatile memory application.

This work was supported by National Science Council, Taiwan, under Project No. NSC 102-2221-E-009-134-MY3.

[1] T. Y. Tseng and S. M. Sze, “An introduction to nonvolatile memories,” in *Nonvolatile Memories: Materials, Devices, and Applications*, edited by T. Y. Tseng and S. M. Sze (Am. Scientific Pub., CA, USA, 2012), Vol. 1, pp. 1–9.
[2] Y. Y. Chen, L. Coux, S. Clima, B. Govoreanu, R. Degraeve, G. S. Kar, A. Fantini, G. Groesenken, D. J. Wouters, and M. Jurczak, IEEE Trans. Electron Devices **60**, 1114 (2013).
[3] B. Gao, B. Sun, H. Zhang, L. Liu, X. Liu, R. Han, J. Kang, and B. Yu, IEEE Electron Device Lett. **30**, 1326 (2009).
[4] B. Gao, J. Kang, L. Liu, X. Liu, and B. Yu, Appl. Phys. Lett. **98**, 232108 (2011).
[5] H.-S. P. Wong, H. Y. Lee, S. Yu, Y. S. Chen, Y. Wu, P. S. Chen, B. Lee, F. T. Chen, and M. J. Tsai, Proc. IEEE **100**, 1951 (2012).
[6] C. Y. Lin, S. Y. Wang, D. Y. Lee, and T. Y. Tseng, J. Electrochem. Soc. **155**, H615 (2008).
[7] Y. Bai, H. Wu, Y. Zhang, M. Wu, J. Zhang, N. Deng, H. Qian, and Z. Yu, Appl. Phys. Lett. **102**, 173503 (2013).
[8] T. Ninomiya, S. Muraoka, Z. Wei, R. Yasuhara, K. Katayama, and T. Takagi, IEEE Electron Device Lett. **34**, 762 (2013).
[9] M. H. Lin, M. C. Wu, C. Y. Huang, C. H. Lin, and T. Y. Tseng, J. Phys. D: Appl. Phys. **43**, 295404 (2010).
[10] D. Y. Lee, T. L. Tsai, and T. Y. Tseng, Appl. Phys. Lett. **103**, 032905 (2013).
[11] J. Lee, E. M. Bourim, W. Lee, J. Park, M. Jo, S. Jung, J. Shin, and H. Hwang, Appl. Phys. Lett. **97**, 172105 (2010).
[12] S. Yu, Y. Wu, Y. Chai, J. Provine, and H.-S. P. Wong, in *2011 International Symposium on VLSI Technology, Systems and Applications (VLSI-TSA)*, 2011, p. 1.
[13] G. H. Kim, J. H. Lee, J. Y. Seok, S. J. Song, J. H. Yoon, K. J. Yoon, M. H. Lee, K. M. Kim, H. D. Lee, S. W. Ryu, T. J. Park, and C. S. Hwang, Appl. Phys. Lett. **98**, 262901 (2011).
[14] W. Shen, R. Dittmann, U. Breuer, and R. Waser, Appl. Phys. Lett. **93**, 222102 (2008).
[15] Y. Lu, B. Chen, B. Gao, Z. Fang, Y. H. Fu, J. Q. Yang, L. F. Liu, X. Y. Liu, H. Y. Yu, and J. F. Kang, in *2012 IEEE International Reliability Physics Symposium (IRPS)* (IEEE, 2012), pp. MY.4.1–MY.4.4.
[16] J. J. Yang, F. Miao, M. D. Pichett, D. A. A. Ohlberg, D. R. Stewart, C. N. Lau, and R. S. Williams, Nanotechnology **20**, 215201 (2009).
[17] B. Chen, J. F. Kang, B. Gao, Y. X. Deng, L. F. Liu, X. Y. Liu, Z. Fang, H. Y. Yu, X. P. Wang, G. Q. Lo, and D. L. Kwong, IEEE Electron Device Lett. **34**, 1292 (2013).
[18] S. Yu, X. Guan, and H.-S. P. Wong, Tech. Dig. -Int. Electron Devices Meet. **2012**, 26.1.1.
[19] J. C. Dupin, D. Gonbeau, P. Vinatier, and A. Levasseur, Phys. Chem. Chem. Phys. **2**, 1319 (2000).
[20] H. Y. Lee, P. S. Chen, T. Y. Wu, C. C. Wang, P. J. Tzeng, C. H. Lin, F. Chen, M. J. Tsai, and C. Lien, Appl. Phys. Lett. **92**, 142911 (2008).
[21] J. K. Lee, S. Jung, J. Park, S. W. Chung, J. S. Roh, S. J. Hong, I. H. Cho, H. I. Kwon, C. H. Park, B. G. Park, and J. H. Lee, Appl. Phys. Lett. **101**, 103506 (2012).
[22] C. S. Kang, H. J. Cho, Y. H. Kim, R. Choi, K. Onishi, A. Shahriar, and J. C. Lee, J. Vac. Sci. Technol. B **21**, 2026 (2003).
[23] S. Y. Wang, D. Y. Lee, T. Y. Tseng, and C. Y. Lin, Appl. Phys. Lett. **95**, 112904 (2009).
[24] H. Choi, J. Yi, S. Hwang, S. Lee, S. Song, S. Lee, J. Lee, D. Son, J. Park, S. J. Kim, J. Y. Kim, S. Lee, J. Moon, C. Kim, J. Park, M. Joo, J. S. Roh, S. Park, S. W. Chung, J. Rhee, and S. J. Hong, in *2011 3rd IEEE International Memory Workshop (IMW)* (IEEE, 2011), pp. 1–4.

This article is copyrighted as indicated in the article. Reuse of AIP content is subject to the terms at: http://scitation.aip.org/termsconditions. Downloaded to IP: 140.113.38.11 On: Fri, 02 May 2014 03:55:39